Reports

Remote Sensing of Ocean Currents

R. M. GOLDSTEIN, T. P. BARNETT, H. A. ZEBKER

A method of remotely measuring near-surface ocean currents with a synthetic aperture radar (SAR) is described. The apparatus consists of a single SAR transmitter and two receiving antennas. The phase difference between SAR image scenes obtained from the antennas forms an interferogram that is directly proportional to the surface current. The first field test of this technique against conventional measurements gives estimates of mean currents accurate to order 20 percent, that is, root-mean-square errors of 5 to 10 centimeters per second in mean flows of 27 to 56 centimeters per second. If the full potential of the method could be realized with spacecraft, then it might be possible to routinely monitor the surface currents of the world's oceans.

MEASURING NEAR-SURFACE OCEAN currents is a difficult task under any circumstances. Conventional current meters give point values whose spatial representativeness is unknown. Shipboard acoustic systems give spatial information, but the data contain time lags and the very near-surface layer is not observed. Drifting buoys can be used to solve the latter problem but the observations obtained from them also can be hard to interpret. We have found that an SAR can be used to provide virtually instantaneous high-resolution snapshots of near-surface currents over large ocean regions (*1*). The basic idea is to use dual antennas to receive the SAR signal and then from the phase difference between the image scenes from the antennas to obtain an interferogram, which is directly proportional to the velocity field of the ocean surface. The method is distinctly different from earlier attempts to use SAR as a remote current meter (*2*) and is an extension of a two-antenna, stationary target–canceling scheme by Raney (*3*).

The main result of our work (Fig. 1) shows the radar-derived estimates of near-surface ocean currents off San Diego, California, compared with more conventional estimates derived from freely drifting "buoys" for approximately the same space-time locations. The two different estimates of surface current are linearly related with a slope of 1.12 ± 0.18 (95% confidence limits), have little bias (2.2 cm/s), and have a root-mean-square (rms) error of 12 cm/s. Well over one-half of the rms error is introduced by just 3 of the 20 data points. Given the experimental limitations discussed below, we believe the agreement between the currents estimated from the SAR interferometer and the buoy observations is quite encouraging.

In our experiment, the interferogram was formed with image scenes from two SAR receivers with their antennas located 19.3 m apart on the National Aeronautics and Space Administration (NASA) DC-8 radar aircraft. Ideally, one antenna should follow collinearly behind the other. If the reflecting elements of the scene were stationary, then the images from the two antennas would be identical except for a displacement along the track. Surface motion, however, produces a phase shift between corresponding picture elements (pixels) of the two images. The phase shift ($\Delta\phi$) is proportional to the change in distance of the resolution element that occurs in the time it takes for the rear antenna to move to a place of symmetry with respect to the front antenna, that is,

$$\Delta\phi = \frac{2\pi B}{\lambda}\frac{u}{v} \qquad (1)$$

where B is the distance between antennas (19.3 m), u is the line-of-sight component

R. M. Goldstein and H. A. Zebker, Jet Propulsion Laboratory, California Institute of Technology, Pasadena, CA 91109.
T. P. Barnett, Climate Research Group, Scripps Institution of Oceanography, La Jolla, CA 92093.

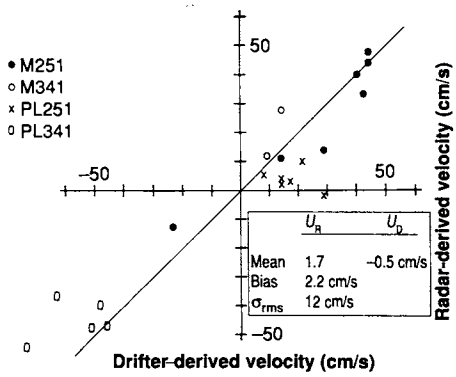

Fig. 1. Scatter diagram for observed versus radar-derived surface currents. The statistics of the data pairs are given in the lower right corner. 'M' and 'PL' refer to data taken off Mission Bay and Point Loma, respectively; the numbers that follow (251 and 341) refer to the current component direction (degrees from true north).

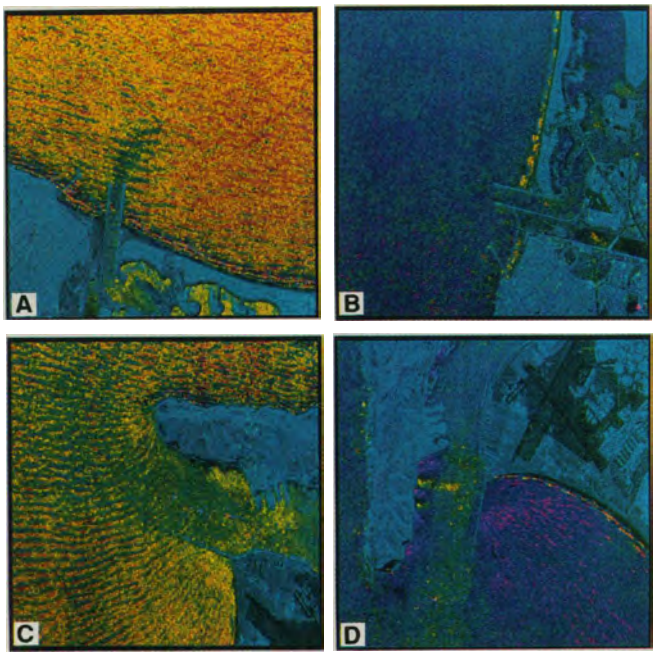

Fig. 2. (**A**) Radar interferogram of the Mission Bay area. Brightness represents echo strength, and hue represents surface motion. The aircraft flight path is from right to left along the top of the figure (toward 161°T). The light blue color of the land represents no motion. The predominantly yellow hue is associated with Bragg waves generated by the prevailing southwest winds that are traveling away from the aircraft. The deep blue streak extending out from the jetties is the outgoing tidal flow (see Fig. 3) and is directed toward the aircraft. The long shore striations are associated with wind wave–induced orbital motions. (**B**) Same as in (A) but for a flight path of 251°T. (**C**) Radar interferogram for Point Loma. The complex surface wave field diffraction around Point Loma is particularly clear in the interferogram but scarcely visible in the conventional SAR image (not shown). (**D**) Same as (B) but for Point Loma. The tidal flow out of San Diego Bay, the yellowest band, is clearly seen, as is the wind wave field and onshore flow (magenta) to the south (right) of Zuniga jetty (see Fig. 4).

of the ocean current velocity, v is the aircraft velocity (220 m/s), and λ is the radar wavelength (0.24 m).

Currents associated with larger gravity waves, internal waves, and other oceanic phenomena are visible to conventional microwave radar only in their ability to modulate the surface Bragg waves (*4*) imaged by the radar. In contrast, our interferometric technique measures the algebraic sum of small displacements of the Bragg waves: the phase velocity of the Bragg waves themselves, the orbital velocity associated with the swell upon which they ride, and any underlying current. Only the line-of-sight component of these velocities is observed.

Our experiment consisted of a flight of the NASA DC-8 radar aircraft from its home base at Moffett Field, California, to the San Diego area and return. The flight reached San Diego at the time of maximum expected outgoing tidal current, near 1230 local daylight time, on 16 April 1988. Radar data were gathered over the outlets of Mission Bay and San Diego Bay from two flight directions each. The directions were chosen to be nearly parallel, and nearly perpendicular, to the expected current directions.

The resulting interferograms are shown in Fig. 2. The first two images (Fig. 2, A and B) are of Mission Bay, as seen from flight directions of 161° (south-southeast) and 251° (west-southwest), respectively. The second two (Fig. 2, C and D) are of Point Loma along the same two flight paths. In these images, radar echo power is portrayed as brightness and phase (Eq. 1) as color. Thus the interferogram is presented coregistered with the conventional SAR image.

The color cyan represents a phase shift of 0° (zero line-of-sight velocity). Motion toward the radar is represented by shades from cyan through violet to magenta, motion away by shades from cyan through green to yellow. In all cases the aircraft flight line is across the top of the figure, toward the left. Most of the surface winds (less than 6 m/s) were from the southwest, producing the yellow bias observed in Fig. 2, A and C, and the violet bias in Fig. 2, B and D. This bias is the result of the phase velocity of the wind-driven Bragg waves.

An extensive wave system can be seen easily in these images, including considerable diffraction around Point Loma. This system is not so easily seen (if at all) in the conventional SAR images. The largest line-of-sight velocity associated with the wave system was 1.5 m/s. In addition to the Bragg wave phase velocity and the larger gravity wave orbital velocity, the outflowing tidal currents can be seen clearly, particularly in Fig. 2, A and D.

We made estimates of the in situ current simultaneously with the radar estimates by observing the motion of the freely drifting buoys (*5*). The buoys were deployed at 15-min intervals in and around the narrowest parts of the entrances to San Diego Bay and Mission Bay (Figs. 3 and 4); this positioning guaranteed that the buoys would likely "see" the largest current signals in the SAR

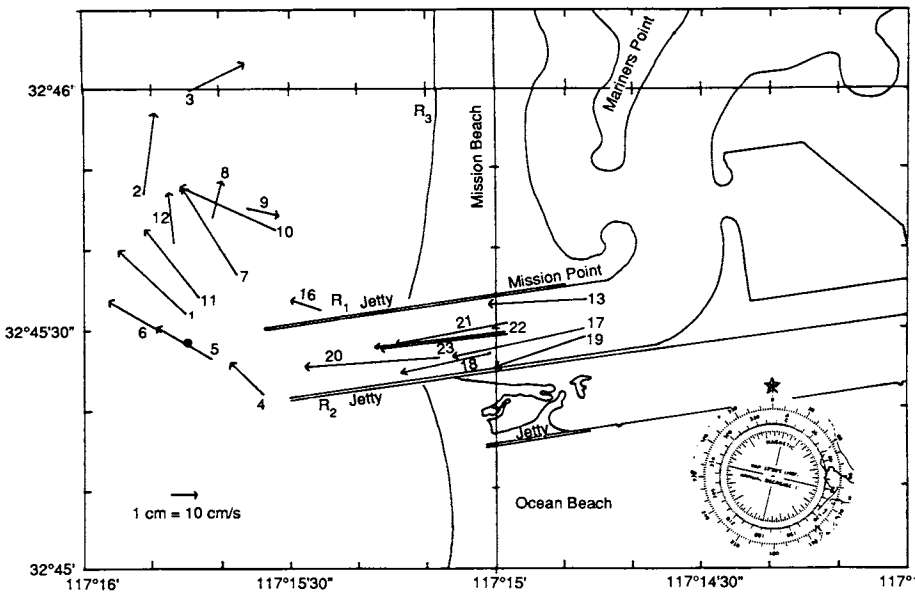

Fig. 3. Observed surface currents around the entrance to Mission Bay, California. The arrows point in the direction of the current, and the length of each arrow is proportional to the observed speed. The letters R_1, R_2, and R_3 designate reference areas for independent estimation of the Bragg wave speed. The solid dot denotes a navigation buoy.

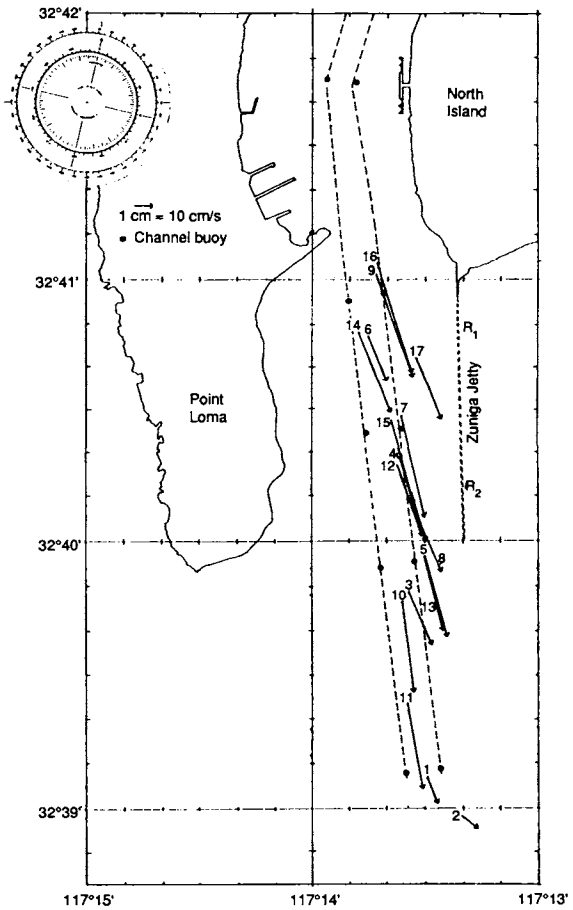

Fig. 4. Same as Fig. 3 but for Point Loma.

images, thus giving the largest signal-to-noise ratio for both current estimates.

The buoys were positioned by Loran-C (long-range navigation) approximately every 15 min. The lorans were on two swift boats and allowed full coverage of the (eventually) extensive buoy arrays at both Point Loma and Mission Bay. Tests of the lorans showed an estimated accuracy for repeat positions to within approximately ± 20 m of a fixed reference, say, a navigation buoy. Typical buoy displacements between positionings were of order 500 m, so current estimates should be accurate to about 4 to 5% or better.

The currents observed by the drifters and radar are tabulated in Table 1. The result of the experiment (the last two columns of Table 1) are shown in Fig. 1. This illustration, Fig. 2, and the associated numerics suggest a number of conclusions:

1) The method is most reliable when one is looking along the direction of strongest flow (Mission Bay, 251°, and Point Loma, 161°).

2) The method seems to be more accurate when one is looking upwind or downwind. In these cases, the Bragg waves responsible for the radar signal are less ambiguous.

3) The estimates of the reference velocity are in relatively good accord with those expected theoretically.

4) The interferograms contain a wealth of information on the ocean wave field and numerous other features in the flow field. We have largely neglected, or processed out, this information in the present study, but the potential of the technique for determination of the surface wave field appears promising.

Using the SAR in the interferometer mode did introduce a problem in our experiment. The collinear condition for the dual antennas was not quite met because of aircraft motion. For example, yaw will cause an effective sideways motion of the antennas, thereby inducing a phase shift and hence making the image scene appear to move even when it is stationary. During the flight over San Diego, the aircraft experienced a good deal of turbulence and so the motion errors were prominent in our data. We corrected for such influences by making use of the aircraft inertial navigation system (INS), which provided frequent readings of pitch, yaw, pitch and yaw rates, horizontal and vertical velocity, and other flight parameters. With the INS data we were able to calculate the expected phase shifts from a stationary field of view and to compensate the measurements accordingly.

We mitigated the effects of the swell first by averaging (filtering) the phase images over a square of 9 by 9 pixels (110 by 110 m on the sea surface). We then averaged the phase over the observed paths of the drifters to make the radar-estimated currents as spatially similar in nature as possible to the directly observed currents. The bias introduced by the Bragg wave phase velocity was estimated for a nearby calm location for which there was little or no tidal current. Theoretically, the value should be 52 cm/s for Bragg waves traveling directly along the line of sight, whereas our calibrated values varied between 50 and 64 cm/s for "look" directions more or less aligned with the wind direction. The modest difference (2 to 12 cm/s) between these values and the theoretical value are measures of the errors inherent in using the INS to correct for plane motion.

The method we have described offers an opportunity for estimating the large-scale ocean surface current field due to the combined effects of tides, wind, and waves on a resolution (12 m) never before obtained. Velocity fields associated with surface waves, internal waves, and Langmuir cells all seem amenable to study with the interferometric technique. On these smaller scales,

Table 1. Radar-derived and observed surface currents (in centimeters per second). Minimum and maximum velocities refer to the 81-pixel averages along the observed path of the drifters. The first column lists the drifter numbers (see Figs. 3 and 4). Average velocities are the grand average over the drifter path. The reference number indicates which area was used to calibrate the Bragg wave phase velocity effect (see Figs. 3 and 4). The resultant radar velocity is the horizontal current velocity near the sea surface in the direction given in the heading. The buoy measurements of the same component are the in situ velocity measurements.

Location number	Velocity			Reference number	Radar velocity	In situ velocity
	Min.	Max.	Average			
			Mission Bay 251° component			
13, 17, 19	−27	−9	−14	*1, 2*	40	40
21, 22, 23	−32	2	−9	*1, 2*	44	44
18	−32	2	−12	*1, 2*	42	33
20	−21	23	−10	*1, 2*	44	48
5,6	−64	11	−28	*1*	29 *2*	14
1, 7, 11	−58	−33	−40	*1, 2*	14	11
2	−88	−53	−73	*2*	−23	13
(R_1)			−57			
(R_2)			−50			
Average					27	25
Bias					2	
rms					8	
			Mission Bay 341° component			
20	−5	23	6	*1*	9	12
2	6	34	21	*3*	14	28
(R_1)			−3			
(R_3)			7			
Average					12	20
Bias					−8	
rms						
			Point Loma 251° component			
9, 16, 17	−55	−40	−50	*1*	14	2
6, 14	−46	−25	−35	*1*	29	−2
4, 7, 12, 15	−47	−40	−44	*2*	17	3
3, 5, 10, 13	−49	−46	−47	*2*	14	4
11	−42	−32	−37	*2*	21	10
2	−56	−46	−53	*2*	8	−5
(R_1)			−64			
(R_2)			−61			
Average					17	2
Bias					15	
rms					7	
			Point Loma 341° component			
9, 16, 17	−38	−14	−29	1	−74	−57
6, 14	−33	−10	−18	1	−63	−45
4, 7, 12, 15	−23	−12	−17	2	−51	−48
3, 5, 10, 13	−23	−9	−14	2	−48	−40
11	−13	−10	−12	2	−46	−48
(R_1)			45			
(R_2)			34			
Average					−56	−48
Bias					−8	
rms					8	
Grand average					1.7	−0.5
Grand bias					2.2	
Grand rms					12	

the problems of aircraft motion will likely be less important than in the present study. This SAR device, if rigged on an orbiting platform, might be subject to fewer problems than experienced on the aircraft. If this were done, the interferometer technique might make feasible the remote sensing of the surface current field for the world oceans.

REFERENCES AND NOTES

1. R. M. Goldstein and H. A. Zebker, *Nature* **328**, 707 (1987).
2. F. I. Gonzales, C. L. Rufenbach, R. A. Shuchman, in *Oceanography from Space*, J. F. R. Gower, Ed. (Plenum, New York, 1981), pp. 511–523.
3. R. K. Raney, *IEEE Trans. Aerosp. Electron. Syst.* **AES-7**, 499 (1971).
4. SAR theory is described in R. Stewart, *Methods of Satellite Oceanography* (Univ. of California Press, Berkeley, 1985), p. 352.
5. Bragg waves observed by the SAR most effectively feel currents at a depth of approximately 2 cm below the mean surface [R. Stewart and J. Joy, *Deep Sea Res.* 21, 1039 (1974)]. We measured these (very) near-surface currents with drifting pieces of plywood (1.2 m long by 0.6 m wide by 2 cm thick) with an identification number on the top. Their overall horizontal dimensions made them rather insensitive to vertical motions of the short waves, whereas their thickness ensured response to the very near-surface currents felt by the Bragg waves. The windage of these simple floats was virtually nil, a fact we checked by droguing several buoys with large, 20-liter, water-filled plastic bags.

6. The research described in this paper was carried out, in part, by the Jet Propulsion Laboratory (JPL) of the California Institute of Technology and was sponsored by JPL and the Defense Advanced Research Projects Agency through an agreement with the National Aeronautics and Space Administration. The University of California Space Institute and the Scripps Institution of Oceanography also sponsored this work. We thank B. and W. Barnett, D. Fuhrman, and A. Saraspe for assisting with the ocean portion of the field program.

17 July 1989; accepted 28 September 1989

Magnitude of Late Quaternary Left-Lateral Displacements Along the North Edge of Tibet

GILLES PELTZER,* PAUL TAPPONNIER, ROLANDO ARMIJO

Images taken by the earth observation satellite SPOT of the Quaternary morphology at 18 sites on the 2000-kilometer-long Altyn Tagh fault at the north edge of Tibet demonstrate that it is outstandingly active. Long-term, left-lateral strike-slip offsets of stream channels, alluvial terrace edges, and glacial moraines along the fault cluster between 100 and 400 meters. The high elevation of the sites, mostly above 4000 meters in the periglacial zone, suggests that most offsets resulted from slip on the fault since the beginning of the Holocene. These data imply that slip rates are 2 to 3 centimeters per year along much of the fault length and support the hypothesis that the continuing penetration of India into Asia forces Tibet rapidly toward the east.

FOR NEARLY 2000 KM, THE ALTYN Tagh fault follows the northwestern edge of the Tibet-Qinghai highlands (Fig. 1). From studies of Landsat images, the fault has been inferred to be active, left-lateral (*1, 2*), and to absorb an important fraction of the present-day convergence between India and Asia by allowing the Tibet-Qinghai plateau to move northeastward relative to the Tarim basin (*1*). Little else is known of this fault, however. The historical seismic record in its vicinity is scanty (*3*). Strike-slip surface breaks have been found in the field only at two localities, near 90° and 96°E (*4*). Estimates of the rate of horizontal slip on the fault vary widely (*5*). Thus, although the length and morphology of the Altyn Tagh fault (*6*) imply that it may be the largest Quaternary strike-slip fault of Asia, further constraints on the amount and history of recent movement are required for a quantitative understanding of recent tectonics north of the Himalayas.

With a pixel size of 10 m in the panchromatic mode, images taken by the satellite SPOT (*7*) allow identification of cumulative Holocene offsets (that is, of features ~10,000 years old) on all faults moving at rates faster than 1 mm per year. In order to measure long-term offsets of late Quaternary morphological features and deposits along the Altyn Tagh fault, we studied seven scenes selected on the basis of earlier work with Landsat (*1*). In these scenes, late Quaternary deformation is spectacular at 18 sites (Fig. 1), 11 of which allow unambiguous estimates of recent left-lateral offsets (Table 1). We describe some of these sites below.

At site 1, the fault trace is marked in abundant, hummocky glacial till. It cuts the valley of a glacier and offsets its lateral moraines (Fig. 2, A and B). The left-lateral offset of the eastern, well-preserved, moraine ridge is 100 ± 20 m. The tip of the present glacier tongue in the valley lies only 1750 m upstream from the fault trace, thus only a few hundred meters above it if the valley slope is 10 to 20% (Fig. 2, A and B).

Between 78° and 79°E, the fault trace lies in the Karakax He valley, for the most part above 4000 m (Fig. 1). Here this valley is a gently west-sloping trough, several kilometers wide, flanked on either side by high mountains, which have been dissected by numerous, mostly extinct valley glaciers (*8*). Streams now flowing down such valleys north of the Karakax have built large alluvial fans. On the SPOT images, the fan deposits appear to form three major terraces, which are cut by the fault trace (Fig. 2, C to F). At site 3 (Fig. 2, C and D), for instance, the edges of the upper and middle terraces on the east bank of the stream are offset left-laterally by 185 ± 20 m. At sites 5 and 6 (Fig. 1 and 2, E and F), two ancient fans are offset 210 ± 20 m and 240 ± 20 m, respectively, in a left-lateral sense. The upper surfaces of these fans are incised by small channels and are no longer depositional surfaces (Fig. 2, E and F). The height of the fan surfaces above the Karakax flood plain and their degree of erosion suggest that they correspond to the middle terrace level at site 3 (Fig. 2, B and D). Close examination of the SPOT image reveals that the fault scarp in the fan surface at site 5 (Fig. 2E) faces toward the north across the eastern half of the fan and toward the south across the western half of this fan (*9*). This geometry, which is also clear across the fan at site 6 and across the terraces at site 3, attests to

Table 1. Values of 15 late Quaternary offsets measured along the Altyn Tagh fault. Errors are taken to be ±2 pixels [pixel sizes are 10 m and 20 m for panchromatic and multispectral (XS) images, respectively] for offsets of sharp, fossil morphological features (for example terrace or moraine edges), and standard deviations for average offsets of stream channels. Approximate elevations of sites, from (*6*), and inferred ages of offsets are also indicated.

Site	Offset (m)	Elevation (m)	Age (10^3 years)
1	100 ± 20	5000	<8
2	175 ± 20	4000	10 ± 2
3	185 ± 20	4000	10 ± 2
	185 ± 20		
5	210 ± 20	4000	10 ± 2
6	240 ± 20	4000	10 ± 2
7	~120	4000	<12
	~250		
	~120		
10	250 ± 80	4600	?
11	195 ± 95	3600	10 ± 2 ?
13	~400	4400	10 ± 2 ?
15	125 ± 40	3500	<8 ?
	125 ± 40		
18	60 ± 40	3300	10 ± 2 ?

Laboratoire de Tectonique, Mécanique de la Lithosphère, Institut de Physique du Globe de Paris, 4, place Jussieu, 75252 Paris, Cedex 05, France.

*Now at Jet Propulsion Laboratory, California Institute of Technology, Pasadena, CA 91109.